Chapter 9
Mechanistic Models with Spatial Structures and Reactive Behavior Change

As we have emphasized in Chaps. 4 and 5, simple homogeneous models of transmission or growth dynamics often yield an early exponential epidemic growth phase even when the population is stratified into different groups (e.g., age, gender, regions). However, recent work has highlighted the presence of early sub-exponential growth patterns in case incidence from empirical outbreak data (Chowell et al. 2016; Viboud et al. 2016). This suggests that integrating detailed and often unobserved heterogeneity into simple mechanistic models (Yan 2018) could open the door to a new and exciting research area to better understand the role of heterogeneity on key transmission parameters, epidemic size, stochastic extinction, the effects of interventions, and disease forecasts.

The diversity of infectious disease dynamics can be shaped by multiple and often unobservable factors including the characteristics of the contact network structure, individual-level heterogeneity in infection risk, and behavior changes (Chowell et al. 2016). For instance, in the simplest setting when disease spreads assuming homogeneous mixing, it is well-known that the incidence curve grows exponentially in the absence of susceptible depletion, behavior changes, and interventions (Diekmann and Heesterbeek 2000). It is worth noting that exponential growth can only unfold in the presence of a constant growth rate (as highlighted in Chaps. 4 and 5). By contrast, an early transmission phase characterized by slower than exponential growth (sub-exponential) can result from spatial constraints in contact-network structures over which disease spreads or the early onset of behavior changes or control interventions. Therefore, predictions of final epidemic size based on models that assume early exponential growth will tend to overestimate epidemic size whenever the early dynamics of disease transmission are governed by mechanisms that induce slower transmission patterns. In turn, public health authorities could get better estimates of the effectiveness of control interventions.

P. Yan, G. Chowell, *Quantitative Methods for Investigating Infectious Disease Outbreaks*, Texts in Applied Mathematics 70,
https://doi.org/10.1007/978-3-030-21923-9_9

We devote this chapter to review mechanistic transmission models that incorporate spatial details or realistic population mixing structures, including metapopulation models, individual-based network models as well as simple SIR-type models that incorporate the effects of reactive behavior changes or inhomogeneous mixing (Fenichel et al. 2011). We argue that designing mechanistic models and statistical approaches that capture a diversity of disease dynamics could lead to enhanced model fit, improved estimates of key transmission parameters, and more realistic epidemic forecasts (Chowell et al. 2016).

Structured population models can be traced back to the 1940s (Wilson and Worcester 1945) and 1950s (Rushton and Mautner 1955). The number of infectious disease spatial modeling studies has been increasing during the last couple of decades with a research production of less than five articles per year in 1997 to more than 120 articles per (Chowell and Rothenberg 2018). Models of the spread of infectious diseases can be formulated at the subpopulation (metapopulation) and individual levels. In metapopulation models the population is divided in a set of interacting population groups according to spatial or demographic characteristics. On the other hand, individual-level network models rely on individual-level contact matrix to define interactions which could be static or dynamic.

9.1 Metapopulation Spatial Models

Metapopulation formulations offer a popular mathematical framework to study the spatial spread of human infectious diseases (Arino et al. 2005; Chowell et al. 2006; Hethcote 2000; Hadeler and Castillo-Chavez 1995; Jacquez 1996; Keeling and Rohani 2008; Sattenspiel 2009). Metapopulation models can be represented as networks with the subpopulations represented by nodes and the interactions among groups represented as the weighted network links (Riley 2007). The subpopulations being modeled using a metapopulation approach are assumed to be discrete groups that are connected in some fashion. Usually subpopulations are considered to be well mixed and homogeneous, while the interaction between groups may be either explicit or implicit, leading to the development of two general classes of spatial metapopulation models: (a) cross-coupled models and (b) mobility models (Sattenspiel 2009). Cross-coupled models simplify the analysis by modeling the strength of the interactions (i.e., coupling) between groups. In mobility models, the modeler mechanistically incorporates the movement of individuals between groups.

Cross-coupled metapopulation models (early examples include Wilson and Worcester 1945; Rushton and Mautner 1955; Murray and Cliff 1977) only model the influence of one group over the others via a contact matrix that represents the strength or sum total of those contacts only. The elements of this matrix capture the strength of the interactions between any two subpopulations, which modulates the transmission risk. A simple SIR deterministic cross-coupled epidemic model can be written as follows:

$$\begin{aligned}
\frac{dS_i}{dt} &= \mu N_i - \mu S_i - S_i \sum_{j=1}^{n} \frac{\phi_{ij} I_j}{N_i} \\
\frac{dI_i}{dt} &= S_i \sum_{j=1}^{n} \frac{\phi_{ij} I_j}{N_i} - (\mu + \gamma) I_i \\
\frac{dR_i}{dt} &= \gamma I_i - \mu R_i,
\end{aligned} \tag{9.1}$$

where S_i, I_i, and R_i are the numbers of susceptible, infectious, and recovered individuals, respectively, N_i is the total population size in subpopulation i, γ is the recovery rate, and μ is the rate of birth (and death) under the assumption of a non-growing population (total births = total deaths). ϕ_{ij} is the rate of effective contact between subpopulation i and subpopulation j; the set of ϕ_{ij} characterizes the WAIFW matrix. The ϕ_{ij} implicitly include both the rate of contact and the probability of transmission.

For illustration, Fig. 9.1 displays the impact of increasing transmission rates of the 4-nearest neighbors on local epidemic simulations using a cross-coupled metapopulation model where 100 local populations each of size 100,000 are spatially arranged in a 10×10 square lattice structure. Perhaps not surprisingly, one can observe how the early local epidemic growth dynamics during the first few generation intervals corresponds well to the epidemic growth derived from a simple SEIR transmission model in a homogenously mixed population. Temporal snapshots of the spatial distribution of disease prevalence using contour plots are shown in Fig. 9.2.

The gravity contact matrix assumes that the rate of contact between two groups is directly proportional to their population size and inversely proportional to their geographic distance (Xia et al. 2004; Viboud et al. 2006; Weinberger et al. 2012). A generalized gravity model takes the form

$$m_{jk} = \frac{N_j^a N_k^b}{d_{jk}^c},$$

where m_{jk} represents the contact between groups j and k, N_j and N_k are the population sizes of the groups, d_{jk} is the distance between the two groups, and a, b, and c are parameters typically estimated from data relating the interactions between the groups.

Recently, Simini et al. (2012) proposed a radiation mobility model. Their model is intended to represent commuting behavior, and they assume that the destinations are determined only by job selection, which is a decision that depends on the size of the location of a specific job opportunity as well as the benefits (e.g., income, working hours, conditions, and other characteristics) of the potential opportunity. Individuals choose the closest job to their home region that has higher benefits than those within the home region. The assigned work locations of all members of a

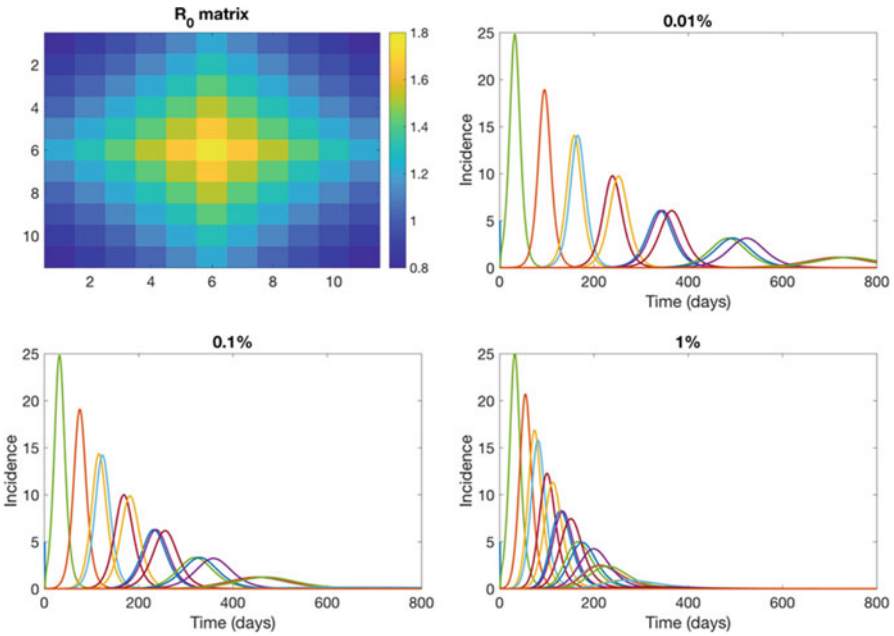

Fig. 9.1 Local epidemics generated using a cross-coupled metapopulation model where 100 local populations are spatially arranged in a 10 × 10 square lattice with periodic boundary conditions. The local dynamics across all patches follow a simple SEIR (susceptible–exposed–infectious–removed) transmission model with a mean latent period of 2 days, a mean infectious period of 3 days, a local basic reproduction number, R0 at 1.5, and a local population size in each patch of 100,000 individuals. A constant transmission between the 4-nearest neighbors is modeled as a fraction of the local transmission rate, which takes values of (a) 0.1%, (b) 0.5%, (c) 1%, and (d) 5%. For reference, the red dotted line corresponds to the curve of total incidence, while the dashed black line corresponds to the solution of the homogenous-mixing SEIR model considering the total homogenously mixed population in a single patch

region determine the daily commuter fluxes. The average flux, T_{ij}, from region i to region j at a distance r_{ij} apart is given by

$$\langle T_{ij} \rangle = T_i \frac{N_i N_j}{(N_i + s_{ij})(N_i + N_j + s_{ij})},$$

where N_i and N_j are the population sizes of regions i and j, respectively, and s_{ij} is the total population in a circle of radius r_{ij} centered on region i but excluding both the source and destination populations. $T_i = \sum_{j \neq i} T_{ij}$ is the total number of commuters who begin their commute in region i. Population distribution is the only required input for this model.

Mobility metapopulation models mechanistically aim to describe the actual movement of individuals across subpopulations (e.g., Arino et al. 2007; Belik et al. 2011; Kenah et al. 2011; Vincenot and Moriya 2011; Xiao et al. 2011; Tizzoni et al.

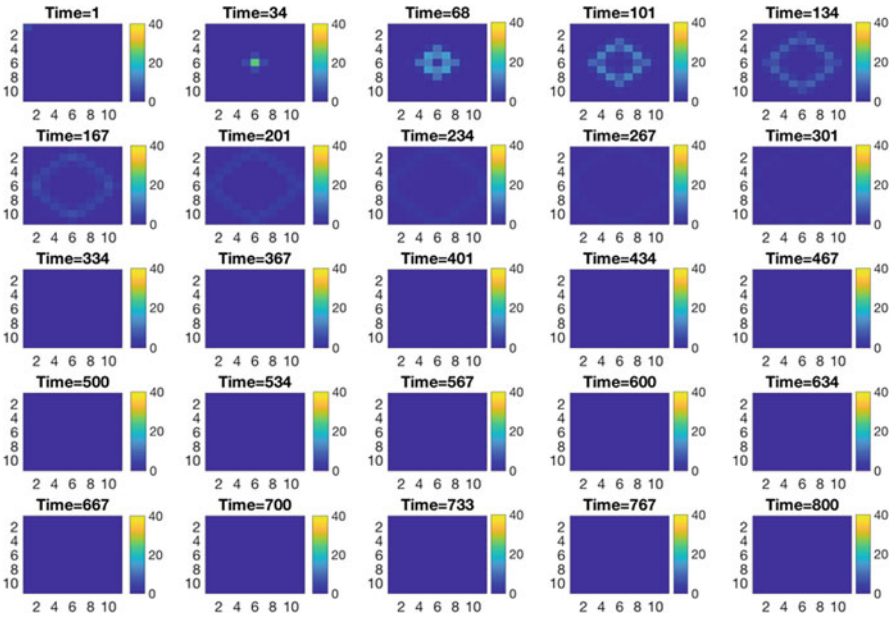

Fig. 9.2 Spatial spread of SEIR metapopulation model in a 10×10 lattice

2012; Appoloni et al. 2013; Apolloni et al. 2014; Marguta and Parisi 2015). Hence, transmission of the pathogen occurs within subpopulations considering the local and visitor populations. This process can also be modeled by considering first the rates at which individuals leave groups to visit other locations and then the possible destinations and average durations of those trips (Sattenspiel and Dietz 1995). An example of a deterministic SIR mobility metapopulation model is the following set of equations:

$$\begin{aligned}
\frac{dS_i}{dt} &= \mu N_i - \frac{\beta_i S_i I_i}{N_i} - \mu S_i + \sum_{j=1}^{n} \theta_{ij} S_j \\
\frac{dI_i}{dt} &= \frac{\beta_i S_i I_i}{N_i} - (\mu + \gamma) I_i + \sum_{j=1}^{n} \theta_{ij} I_j \\
\frac{dR_i}{dt} &= \gamma I_i - \mu R_i + \sum_{j=1}^{n} \theta_{ij} R_j,
\end{aligned} \tag{9.2}$$

where S_i, I_i, and R_i are the numbers of susceptible, infectious, and recovered individuals, respectively, and N_i is the total population size of subpopulation i, μ is the rate of birth (and death) where total births = total deaths, β_i is the transmission parameter in subpopulation i, and θ_{ij} is the rate of movement to subpopulation i

from subpopulation j. Moreover, rates of movement are assumed to be the same for all disease states in this simple model.

9.2 Individual-Based Network Models

Individual-level network models are being increasingly used to study infectious disease dynamics where contacts (links) can be either static or dynamic (reviewed in Halloran et al. 2002; Keeling and Eames 2005; Bansal et al. 2007; Capaldi et al. 2012; Danon et al. 2011). A contact-network model explicitly represents host interactions that dictate disease transmission. A node in a contact network represents an individual host, and an edge between two nodes represents an interaction through which infection is possible. Network-based models are then useful for investigating the impact of individual-level characteristics and their disease-relevant interactions on the transmission dynamics observed at the population level. A number of network models have been proposed in the literature ranging from random, small-world, to scale-free networks (Watts and Strogatz 1998; Barabási and Albert 1999; Albert and Barabasi 2002). One of the most popular and parsimonious contact-network models is the "small-world" network model as it allows for tuning the average degree of the nodes, the average connectivity (path length), and the clustering that quantifies the extent to which contacts of a node are also contacts of each other (Watts and Strogatz 1998).

Figure 9.3 shows two small-world networks with two different rewiring probabilities. While the original Watts–Strogatz model starts from a ring network structure, the idea can be extended to other regular networks. For instance, Fig. 9.4 displays examples of small world networks based on two dimensional lattices where

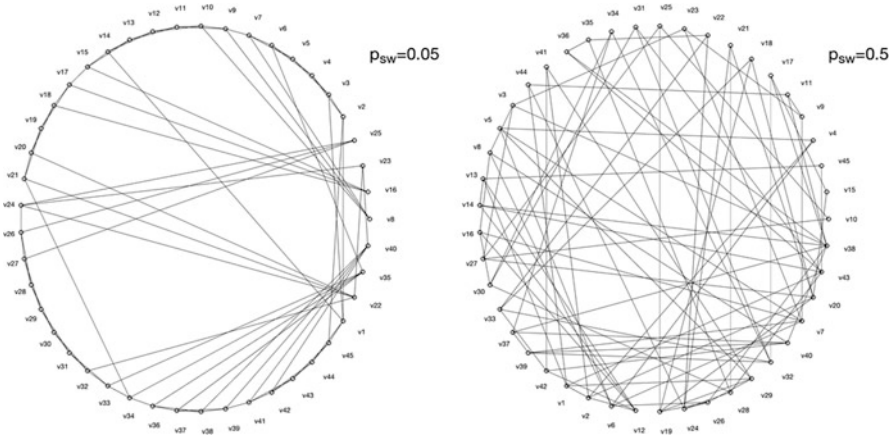

Fig. 9.3 Small-world networks with two rewiring probabilities

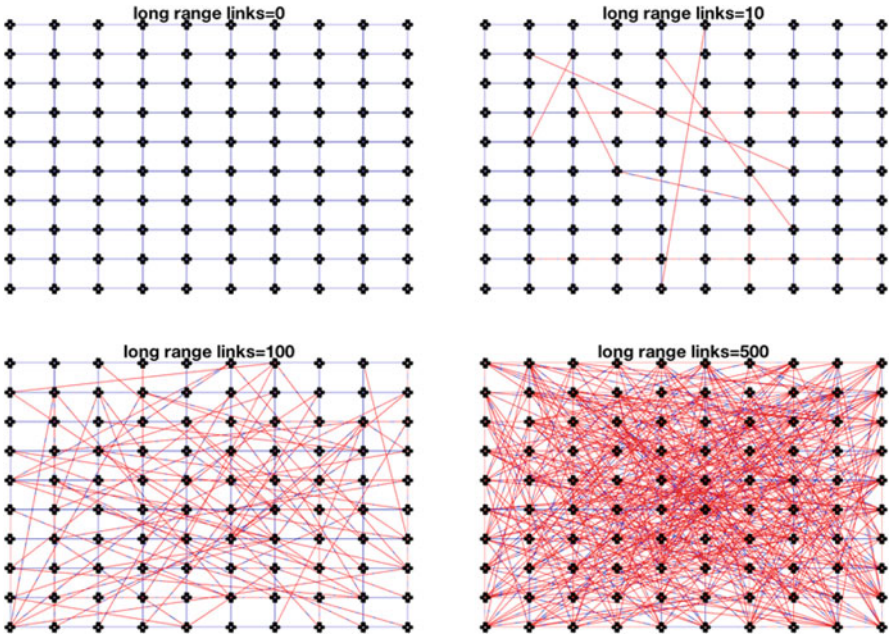

Fig. 9.4 Schematic representation of 2D square lattices where each node is connected to its 4-nearest neighbors with periodic boundary conditions and with the addition of a few random long-range links

each node is connected to its 4 nearest neighbors, and the small-world feature is incorporated by adding a fixed number of random links.

For illustration, we simulated SIR (susceptible–infectious–removed) dynamics on small-world networks using networks of size $N = 90{,}000$ and node connectivity to the 4 nearest neighbors, and we increased the edge rewiring probability parameter (p_{sw}) from 0.001 to 0.01 of the small-world network model of Watts and Strogatz (1998). For each value of p_{sw}, we analyzed the early epidemic growth profile comprising 35 days of disease transmission from 200 stochastic realizations. The transmission rate per contact per unit of time was set at 2 and the infectious period was assumed to be exponentially distributed with mean $1/\gamma$ which is set at 3 days. Each simulation started with one infectious individual selected at random from the network. For reference, the baseline SIR transmission dynamics on the regular network with node connectivity to the 4 nearest neighbors and without long-range links correspond to a wave of steady case incidence at about 4 cases per day.

9.2.1 An Individual-Level Network Model with Household-Community Structure

One of the putative mechanisms leading to early polynomial growth dynamics of transmission is clustering (Szendroi and Csányi 2004; Chowell et al. 2015; Merler et al. 2015; Viboud et al. 2016; Chowell et al. 2017), a network property that quantifies the extent to which the contacts of one individual are also contacts of each other (Watts and Strogatz 1998). Social contact networks are particularly useful to explore the impact of clustering and play an important role in the dissemination of infectious diseases at the community level.

Several authors have put forward relatively simple mathematical models that incorporate household and other social structures such as schools and workplaces (Longini and Koopman 1982; Longini et al. 2007; Ball et al. 2009, 2015; Fraser 2007; Goldstein et al. 2009; Pellis et al. 2009, 2012, 2015; Blythe and Castillo-Chavez 1989). For instance, a network-based transmission model with household structure embedded in a structure of overlapping communities has been previously applied to study the transmission dynamics of Ebola (Kiskowski 2014; Kiskowski and Chowell 2015). In this model, individuals are organized within households of size H (each household contains H individuals) and households are organized within communities of size C households (each community contains $\times$ H individuals) (see Fig. 9.5). Network connectivity is identical for every individual. The transmission potential is characterized by the household reproduction number and the community reproduction number. For a given household size H, prior studies have investigated

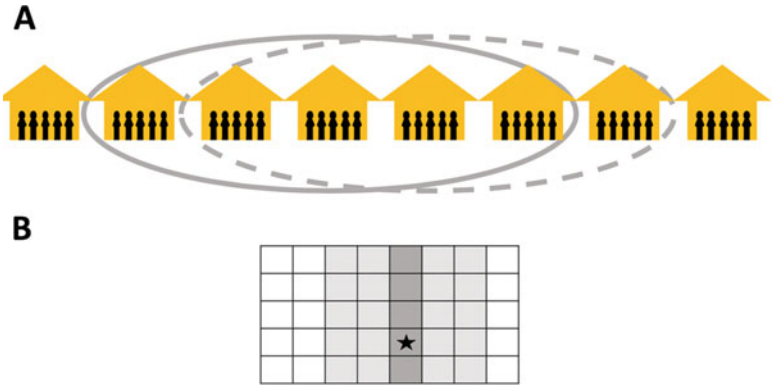

Fig. 9.5 Schematic representation of the household-community mixing structure with overlapping communities. In this model, individuals are organized within households of size H (each household contains H individuals) and households are organized within communities of size C households (each community contains $\times H$ individuals) (panel (**a**)). Network connectivity is identical for every individual. The transmission potential is characterized by the household reproduction number and the community reproduction number. The matrix-level representation of the model is shown in panel (**b**)

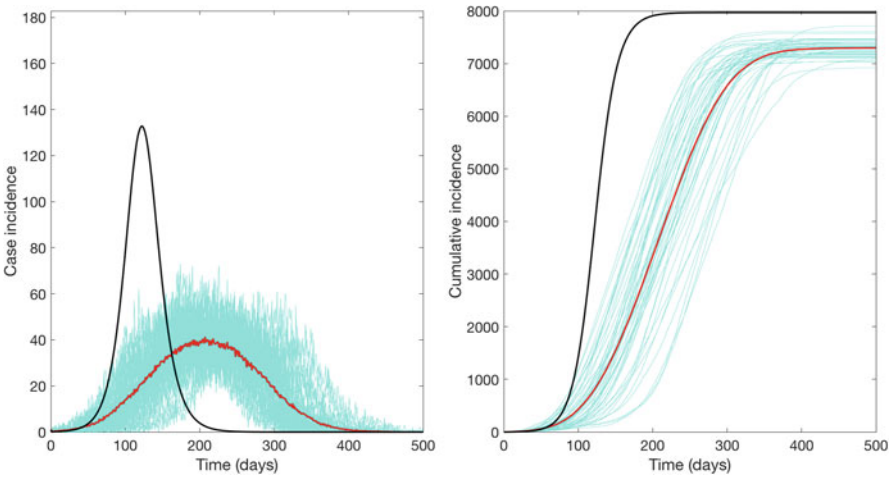

Fig. 9.6 Stochastic SEIR simulations (cyan lines) of the household-community model with $H = 6$, $C = 165$, and $R_{0H} = 1.5$ and $R_{0H} = 0.5$. The mean of the ensemble of stochastic realizations is the red solid line. The corresponding solution of the deterministic SEIR model under homogenous mixing with $R_0 = 2$ corresponds to the solid black line. Baseline epidemiological parameters were set according to the epidemiology of Ebola (i.e., incubation period of 5 days (Eichner et al. 2011; The World Health Organization Emergency Response Team 2014) and infectious period of 7 days (Chowell et al. 2004; The World Health Organization Emergency Response Team 2014)). The population size at 10,000

the impact of varying the community size parameter C on the early transmission phase. As the community size increases, the scaling of epidemic growth approaches the exponential growth regime (Kiskowski and Chowell 2015; Chowell et al. 2016). Figure 9.6 contrasts simulations derived from the household-community model with the deterministic solution of the SEIR model under homogenous mixing with the same R_0. In particular, outbreaks not only spread more slowly in the spatial household-community model, but the size of those epidemics is smaller compared to the homogenous mixing SEIR model using baseline epidemiological parameters (mean latent and infectious periods) in line with the epidemiology of Ebola.

9.3 Capture Dynamic Reactive Behavior Changes Through a Generalized-Growth SEIR Model

The generalized-growth SEIR model (GG-SEIR) is a novel modeling framework (Chowell et al. 2016) that builds on the well-known SEIR (susceptible–exposed–infectious–recovered) transmission model (Anderson and May 1991) by incorporating flexible early epidemic growth profiles, e.g., sub-exponential and exponential growth dynamics. This is achieved by allowing a dynamic nature of the effective

reproduction number R_t in the context of early sub-exponential (e.g., polynomial) growth dynamics.

The standard deterministic SEIR epidemic model represents the simplest and most popular mechanistic compartmental model for describing the spread of an infectious agent in a well-mixed population. As explained before, the force of infection per unit of time is simply given by the product of three quantities: a constant transmission rate (β), the number of susceptible individuals in the population ($S(t)$), and the probability that a susceptible individual encounters an infectious individual ($I(t)/m$). Moreover, infected individuals experience a mean latent and a mean infectious period given by α^{-1} and γ^{-1}, respectively. The model is based on a system of ordinary differential equations that keep track of the temporal progression in the number of susceptible, exposed, infectious, and removed individuals (see Eq. (5.53)).

In a completely susceptible population, e.g., $S(0) = m$, the average number of secondary cases generated per primary case, $R_0 = \beta/\gamma$. However, as the number of susceptible individuals in the population declines due to a growing number of infections, the effective reproduction number over time, R_t, is given by the product of and the proportion of susceptible individuals in the population:

$$R_t = \frac{\beta}{\gamma}\frac{S(t)}{m}. \tag{9.3}$$

During the first few generations of disease transmission when $S(t) \approx m$, in the absence of control interventions or reactive population behavior changes, the standard SEIR model supports a reproduction number that is essentially invariant, i.e., $R_t \approx R_0$. By contrast, in the context of epidemics characterized by early sub-exponential growth dynamics, we have shown that the reproduction number is a dynamic quantity that declines over disease generations towards 1.0 (Chowell et al. 2016). Here we introduce the generalized-growth modeling framework based on the well-known SEIR model (GGM-SEIR) that incorporates the possibility of early sub-exponential growth dynamics by explicitly modeling the dynamic behavior of the effective reproduction number via a time-dependent transmission rate $\beta(t)$ such that the force of infection becomes: $\beta(t)S(t)I(t)/m$. Specifically, we consider a transmission rate function $\beta(t)$ of the form:

$$\beta(t) = \beta_0 \left[(1-\phi)\, f(t;\Theta) + \phi\right],$$

where $f(t;\Theta)$ is a function that declines over time from 1 towards zero so that the transmission rate $\beta(t)$ declines from an initial value β_0 towards $\phi\beta_0$. The quantity $(1-\phi)$ models the proportionate reduction in β_0 that is needed to reach an effective stationary reproduction number at 1.0, in line with early sub-exponential growth dynamics (Chowell et al. 2016). For the standard SEIR model, ϕ can be simply estimated as γ/β_0 since $R_0 = \beta/\gamma$ during the early growth phase when $S(t) \approx m$.

Here we employ an exponential decline function for the transmission rate, which is given by

$$\beta(t) = \beta_0 \left[(1-\phi)\, e^{-qt} + \phi\right],\ 0 < q \leq 1 \text{ and } \phi > 1.$$

Alternatively, harmonic and hyperbolic functions could be used to model the decline in the transmission rate as follows:

$$\beta(t) = \beta_0 \left[(1-\phi)\,(1+qvt)^{-1} + \phi\right],$$

$$\beta(t) = \beta_0 \left[(1-\phi)\,(1+qvt)^{-1/v} + \phi\right].$$

This modeling framework allows to capture early sub-exponential growth dynamics whenever $R_0 > 1$ and $q > 0$. If $q = 0$, the transmission rate $\beta(t) = \beta_0$ remains at the baseline value, and we recover the classic SEIR transmission model with exponential growth dynamics and $R_0 = \beta/\gamma$. In general, the higher the value of q, the faster the decline of the reproduction number from $R_0 > 1$ to a stationary reproduction number at 1.0. We can interpret the parameters q and v through the half time value or the average time elapsed to achieve a transmission rate $\frac{1}{2}\beta_0\,(1-\phi)$. The half time value is given by: $\log(2)/q$.

Importantly, in the context of early sub-exponential (e.g., polynomial) epidemic growth for which $q > 0$, the basic reproduction number is no longer the product of the initial transmission rate β_0 and the mean infectious period γ^{-1} because the transmission rate $\beta(t)$ is no longer constant, but declines during the duration of the infectious period of primary cases at the onset of the epidemic, yielding a lower R_0. For this situation, R_0 can be estimated numerically using the following integral equation (Bacaër and Ait Dads el 2011):

$$R_0 = \int_0^\infty \beta(t) e^{-\gamma\tau} d\tau = \int_0^\infty \beta_0 \left[(1-\phi)\, e^{-q\tau} + \phi\right] e^{-\gamma\tau} d\tau.$$

For a given value of β_0 and γ, the basic reproduction number is R_0 expected to decline from β/γ as parameter q increases above 0. More generally, the effective reproduction number, R_t, during the early epidemic growth phase comprising the first few disease generations of transmission when $S(t) \approx m$ can be numerically computed as follows:

$$R_t = \int_t^\infty \beta(t) e^{-\gamma(\tau-t)} d\tau = \int_t^\infty \beta_0 \left[(1-\phi)\, e^{-q\tau} + \phi\right] e^{-\gamma(\tau-t)} d\tau.$$

For illustration, Fig. 9.7 displays temporal profiles of the transmission rate, the effective reproduction number, and the corresponding simulations of the early epidemic growth phase.

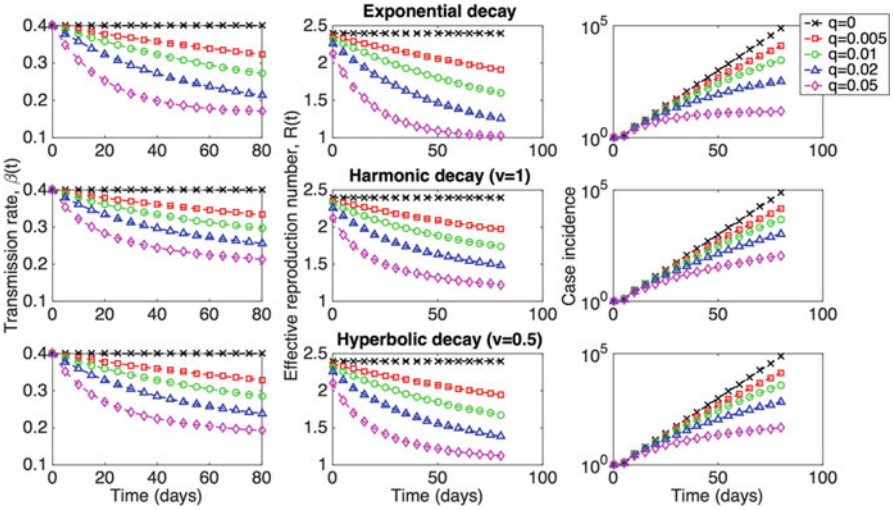

Fig. 9.7 Representative profiles of the transmission rate $\beta(t)$, the effective reproduction number R_t, and corresponding simulations of the early epidemic growth phase derived from the generalized-growth SEIR model (GG-SEIR) for different values of the decline rate parameter q and $\beta_0 = 0.4$,$\alpha = 1/5$, and $\gamma = 1/6$ in a large population size ($N = 10{,}000{,}000$). The epidemic simulations start with one infectious individual. In semi-logarithmic scale, exponential growth is evident if a straight line fits well several consecutive disease generations of the epidemic curve, whereas a strong downward curvature in semi-logarithmic scale is indicative of sub-exponential growth. Our simulations show that case incidence curves display early sub-exponential growth dynamics even for very low values of q

9.4 Case Study: Modeling the Effectiveness of Contact Tracing During Ebola Epidemics

In Mali, two Ebola cases were imported from neighboring Guinea in two different instances, the first resulting in one death and no local secondary cases, and the second resulting in two generations of transmission with a total of eight cases and six deaths in the capital city of Bamako (Breakwell et al. 2016). Both Ebola importations occurred in the fall of 2014 as the epidemic was still unabated in Guinea (2015, 2016), about a month after an Ebola case was imported to Senegal from Guinea, and 4 months after an Ebola case was imported to Nigeria from Liberia (Abdoulaye et al. 2014; The World Health Organization 2014). No further Ebola importations were reported from highly affected countries to neighboring, high-risk countries during the 2014–2016 West Africa Ebola epidemic.

The second Ebola importation in Mali occurred in a grand Imam who traveled from Guinea to Mali and sought care at a private clinic on October 25, 2014, in Bamako where he was treated for kidney failure and was not suspected with Ebola. He died on October 27th and had an unsecured burial on October 28th. Control measures in Mali, including contact tracing, began on November 8th 2014 (Breakwell et al. 2016).

Contact tracing was the primary intervention in response to the second Ebola importation into Mali. Briefly, contact tracing is a method used to prevent further cases of an infectious disease that involves contacting and routinely following up with individuals who have been identified as being exposed to a patient or other vector of a disease for the duration of the maximum observed incubation period of the disease (21 days for Ebola (Shrivastava et al. 2014)). Through effective contact tracing, secondary cases are quickly isolated to prevent further transmission (Eames and Keeling 2003). Although contact tracing is a critical piece of a response to Ebola outbreaks, it was implemented with varying levels of effectiveness across all three of the most affected countries in West Africa (Pandey et al. 2014; Martín et al. 2016; Olu et al. 2016). The success of contact tracing is tightly linked to behavioral interventions, training in infection prevention and control practices in healthcare settings, and initiation of surveillance protocols (Breakwell et al. 2016).

In this case study, we analyze the relation between contact tracing activities and the decline in disease transmission during the Ebola epidemic in Mali. For this purpose, we carried out a comprehensive analysis of contact tracing trees and modeled the relationship between the time-dependent effects of contact tracing and the trajectory of the Ebola outbreak in Bamako assuming two different population structures: (1) a standard homogenous mixing model and (2) a spatially structured model. We illustrate the effect of the rapid and effective implementation of contact tracing activities on outbreak trajectory and size using stochastic simulations.

9.4.1 Model 1: Homogenous-Mixing SEIR Transmission Model

The main features of this model have been described in previous chapters (see Sect. 5.4). A similar model has been previously used to model transmission and control of the Ebola outbreak in Nigeria in 2014 (Chowell et al. 2004; Fasina et al. 2014). For the sake of simplicity, we only model a single infectious compartment while adjusting the time-specific transmission rate according to data of the time-dependent effectiveness in contact tracing activities conducted during the Ebola outbreak in Bamako. Hence, the modeled population was divided into five categories: susceptible individuals (S); exposed individuals (E); infectious and symptomatic individuals (I); and recovered or dead individuals (R). Susceptible individuals infected through contact with infectious individuals enter the latent stage at mean rate $\beta f(t) I(t)/N(t)$, where β is the baseline mean human-to-human transmission rate per day in the absence of interventions, $f(t)$ quantifies the time-dependent effectiveness of contact tracing activities, and $N(t)$ is the total population size at time t. Thus, $f(t)$ ranges from 0 (fully complete contact tracing activities are in place) to 1 (contact tracing efforts are yet to start) to quantify the effectiveness of the isolation of infectious individuals that decrease Ebola transmission through contact tracing efforts. Values of $f(t)$ close to 0 illustrate "near-perfect" contact

tracing, while values closer to 1 illustrate "imperfect" contact tracing efforts. Symptomatic infectious individuals $I(t)$ recover at the mean rate γ. Individuals in the "removed" category do not contribute to the transmission process. Thus, the time-dependent contact tracing effectiveness, $f(t)$, remains at 1.0 before the start of contact tracing activities. Baseline epidemiological parameters were set according to the epidemiology of Ebola (i.e., incubation period of 5 days (Eichner et al. 2011; The World Health Organization 2014) and infectious period of 7 days (Chowell et al. 2004; The World Health Organization 2014)). We set the effective population size at 2,400,000 based on the population size of Bamako. For this model, R_0 is given by the product of the transmission rate β and the mean infectious period $1/\gamma$. Hence, specific values of R_0 (range: 1.6–2.0 based on estimates of the Western African outbreak (Althaus 2014; Nishiura and Chowell 2014)) were calibrated by tuning β. Once interventions are put in place, the effective reproduction number declines according to the formula

$$R_t = R_0 \frac{S(t)}{m} f(t),$$

where $S(t)/m$ quantifies the proportion of susceptible individuals at time t.

9.4.2 *Model 2: Spatially Structured Ebola Transmission Model*

One of the putative mechanisms leading to early polynomial growth dynamics of Ebola transmission is clustering (Szendroi and Csányi 2004; Chowell et al. 2015; Merler et al. 2015; Viboud et al. 2016; Chowell et al. 2017), a network property that quantifies the extent to which the contacts of one individual are also contacts of each other (Watts and Strogatz 1998). Social contact networks are particularly useful to explore the impact of clustering and play an important in the dissemination of Ebola at the community level. We employ a network-based transmission model with household-community structure, which has been previously applied to study the transmission dynamics of Ebola (Kiskowski 2014; Kiskowski and Chowell 2015).

In this model, individuals are organized within households of size H (each household contains H individuals) and households are organized within communities of size C households (each community contains $C \times H$ individuals). Network connectivity is identical for every individual. The household reproduction number R_{0H} was varied between 1.6 and 2.0 and the community reproduction number R_{0C} was set at 0.7 based on previous study (Kiskowski and Chowell 2015). For a fixed household size at $H = 6$, which is in line with the average household size for Bamako in 2014 and various values of the community size parameter (range: 25–65 households per community), we analyze the resulting outbreak size distribution.

9.4.3 *Modeling the Time-Dependent Effectiveness of Contact Tracing Efforts in Bamako, Mali*

After the start of the interventions at time t_0, the function $f(t)$ modulates a decline in transmission rate according to the time-dependent completeness of contact tracing efforts. The functional form for $f(t)$ was assumed to follow an exponential decline after the start of contact tracing activities. That is,

$$f(t) = \begin{cases} 1, & 0 < t < t_0 \\ 1 - (1 - e^{-q(t-t_0)}), & t \geq t_0 \end{cases}.$$

Parameters q and t_0 could be estimated by fitting $f(t)$ to the daily contact tracing completeness calculated as the daily proportion of contact persons that were monitored out of the total number of registered contact persons at risk. For illustration purposes, we set $q = 0.14$ while the start of contact tracing efforts is fixed at $t_0 = 21$, which is in line with the outbreak response in Mali. The corresponding estimates of the effective reproduction number are shown in Fig. 9.9b.

Stochastic Simulations

To assess the temporal and size distribution of outbreaks, we generated 200 stochastic epidemic simulations that start with the introduction of the index case (i.e., $I(0) = 1$). Simulation code in Matlab is available upon request from the authors.

In the absence of interventions, the spatial and non-spatial models exhibit strikingly different epidemic trajectories as shown in Fig. 9.8.

The resulting curves of the effective reproduction number, R_t, capturing the time-dependent effects of contact tracing efforts for three different values of R_0 are shown in Fig. 9.9 based on the homogeneous mixing model. R_t declined below the epidemic threshold of 1.0 between November 10th and November 13th, 2014. The illustrated effect of control interventions on the transmission of Ebola in Mali is shown with an ensemble of stochastic epidemic realizations in Fig. 9.9a, which shows the relative reduction in the transmission rate as a function of the time-dependent effectiveness of contact tracing activities. After the start of the interventions, the function modulates a decline in transmission rate according to the time-dependent effectiveness of contact tracing efforts as explained in the text. This time-dependent function was assumed to follow an exponential decline after the start of contact tracing activities. Figure 9.9b shows the effective reproduction number over time reflecting the impact of contact tracing activities for three different

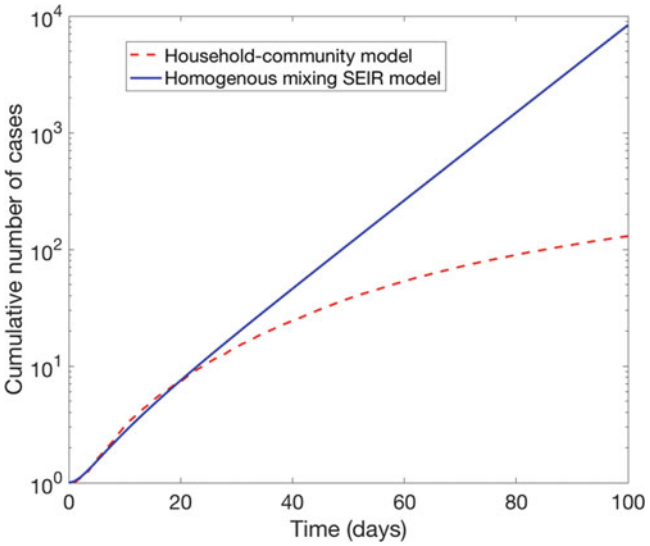

Fig. 9.8 The mean epidemic trajectories derived from the spatial and non-spatial models during the first 100 days of the Ebola epidemic in the absence of interventions

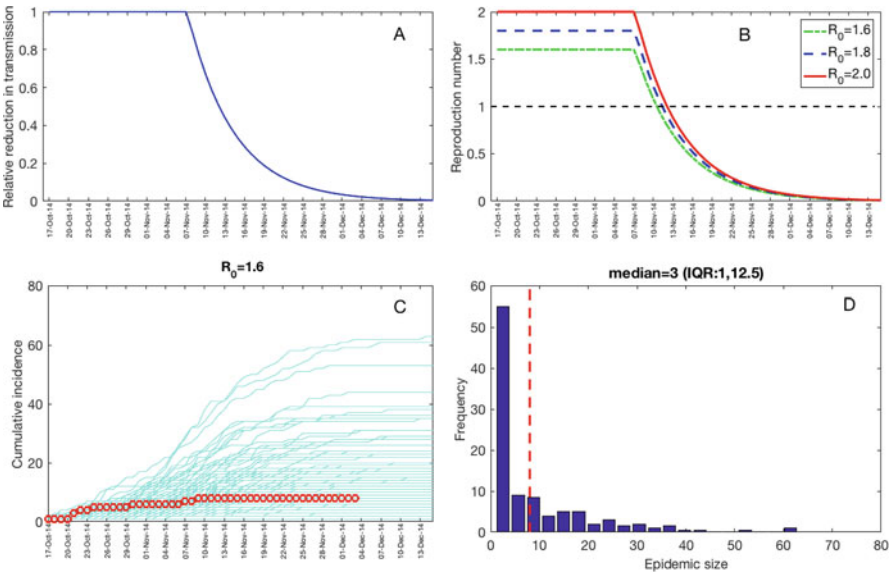

Fig. 9.9 (**a**) The relative reduction in the transmission rate as a function of the time-dependent effectiveness of contact tracing activities. (**b**) The effective reproduction number over time reflecting the impact of contact tracing. (**c**) Stochastic epidemic realizations using the homogenous-mixing SEIR model (Model 1) at $R_0 = 1.6$. The red circles correspond to the actual outbreak trajectory and the cyan blue lines correspond to 200 stochastic realizations. (**d**) The corresponding distribution of outbreak sizes using the homogenous-mixing SEIR model (Model 1) with an R_0 set at 1.6. The vertical dashed line indicates the actual Ebola outbreak size in Mali

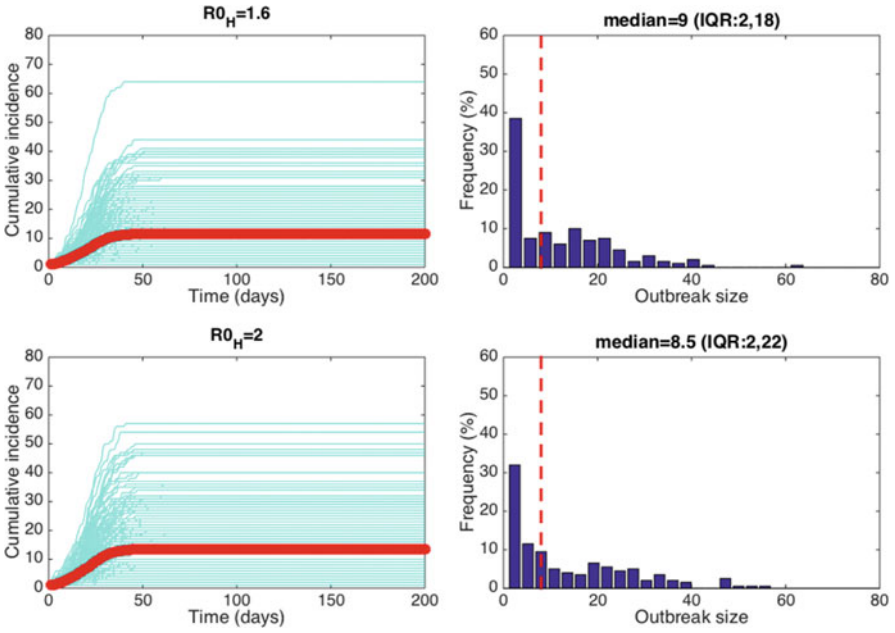

Fig. 9.10 Stochastic epidemic realizations using the household-community SEIR model (Model 2) with a community size of 25 households and household size of 6 which is in line with the average household size for Bamako in 2014

values of R_0 in the range 1.6–2.0. Figure 9.9c illustrates stochastic epidemic realizations using the homogenous-mixing SEIR model (Model 1) with an R_0 set at 1.6. Figure 9.9d shows the corresponding distribution of outbreak sizes using the homogenous-mixing SEIR model (Model 1) with an R_0 set at 1.6. The corresponding results based on the spatially structured model are shown in Fig. 9.10 assuming a community size $C = 25$.

Our modeling analysis demonstrates that the decline in transmission and subsequent halting of the Ebola outbreak in Mali coincided with the implementation of contact tracing activities that improved over the course of the outbreak. The results suggest that contact tracing done completely during an outbreak could minimize the size of future outbreaks. While the spatial and non-spatial models yield significantly different epidemic trajectories in the absence of interventions (Fig. 9.8), it is perhaps not surprising that the spatial and non-spatial transmission models yielded similar outbreak size distributions because the virus was contained before it could spread beyond a few generations of disease transmission. In the absence of comprehensive contact tracing efforts, person-to-person transmission of Ebola could have increased rapidly, ensuing in a sizable urban epidemic.

9.5 Problems and Supplements

9.1 Consider a simple SIR model with an $R_0 = 1.8$, a mean infectious period of 3 days and a population size of 100,000 people that incorporates the effects of behavior changes that mitigate the transmission rate as follows: After the first 30 days of the epidemic, the transmission rate decreases exponentially fast with a half-life of 10 days. Answer the following questions:

(a) Compare the size of the epidemics obtained with and without the effects of behavior changes.
(b) Explore how the epidemic size changes as you vary the timing of the start of the behavior change and the half-life of the transmission rate decay associated with the behavior change.

9.2 Consider a simple two-patch SEIR model with local $R_0 = 1.5$, mean latent period of 7 days, mean infectious period of 4 days, and a population size of 10,000 people in each patch. Further, transmission can occur in two different ways: (1) local transmission within each patch and (2) directed transmission from the first patch to the second patch (but not from the second to the first patch) where this patch-to-patch transmission rate is a fraction ρ relative to the local transmission rate. Answer the following questions:

(a) Using the simple SEIR model without demographic factors and assuming a mean latent period of 2 days, a mean infectious period of 4 days, and a population size of 550,000, provide the mean estimate and 95% confidence intervals of the basic reproduction number R_0 using 16, 18, and 20 days of the initial growth phase. For parameter estimation you can use the least square fitting approach with the Poisson parametric bootstrap which is described in Chap. 7 and illustrated with examples in Chap. 8. Note that you only need to estimate the transmission rate using your favorite technical computing language while keeping the initial number of infectious individuals $I(0)$ fixed according to the first data point. Are the R_0 estimates relatively stable during the study period?
(b) Describe the dynamics of the epidemics as the parameter rho is increased from 0.00001 to 0.01. In particular, how many peaks do the total incidence curve exhibit as this parameter is varied?
(c) Describe the epidemic duration and size that result from (a).
(d) Repeat the analyses in (a) using a system of 4 patches connected in a linear fashion where patch-to-patch transmission only occurs from patch j to patch $j + 1$.